INTENSITY–FREQUENCY DEPENDENCE OF THE RADIO SKY BACKGROUND

By K. W. YATES* and R. WIELEBINSKI*

[*Manuscript received December* 22, 1965]

Summary

Measurements of sky intensity have been made at the frequencies 14·1, 20, 30, 48·5, and 85 MHz with scaled aerials of low resolution directed towards declination $\delta = -34°$. The measurements were carefully calibrated in terms of thermal resistors. Ionospheric effects were eliminated by planning of observations.

The observational data are analysed, on the basis of two different galactic models, to give limiting values for the spectral index of galactic emission and the magnitude of the extragalactic component of the total emission.

I. INTRODUCTION

The law of variation of radio brightness with wavelength is of fundamental importance as a starting point in setting up models of galactic emission mechanisms. This law is characterized by the dependence $B \propto \lambda^{\alpha}$, where B represents the brightness or flux density per unit solid angle, measured in W m^{-2} Hz^{-1} sr^{-1}, and α is the power spectral index. The temperature spectral index β at radio frequencies is defined by the relation

$$T \propto \lambda^{\beta};$$

further,

$$\beta = \alpha + 2.$$

The collection and interpretation of the absolute radio intensity data necessary for the determination of the spectral law is, however, difficult. Even if we assume perfect measurement technique, it is necessary to distinguish the effects of several different phenomena on the total power received. For a broad-beam antenna directed at the sky, these phenomena include thermal and non-thermal emission from the Galaxy, absorption in ionized hydrogen clouds local to the Sun, an integrated component of emission from point sources beyond the Galaxy, and absorption in the ionosphere.

To be directly comparable, intensity measurements for the determination of the spectral law must be made with aerials that are exactly scaled with wavelength. This limits the size of the antennas and, hence, the beamwidth. Comparison of surveys made with different aerials could give the spectral index, but in practice it is not possible to compute or measure aerial patterns to the degree of accuracy required. Scaled aerial experiments have been made by Adgie and Smith (1956), Costain (1960), Turtle *et al.* (1962), Korobkov (1964), Ellis (1965), and Parthasarathy and Lerfald (1965), aimed at determining the spectral index variation in the metre and decametre range of wavelengths. A summary of these experiments is presented

* School of Electrical Engineering, University of Sydney.

TABLE 1

SCALED AERIAL RADIO INTENSITY MEASUREMENTS IN THE METRE AND DECAMETRE RANGES OF WAVELENGTHS

Observer	Declination (deg)	Beamwidth	Observations (MHz)	f (MHz)	β	Direction	Method of Analysis
Turtle *et al.* (1962)	+50	44° by 15°	404, 178, 38, 26	40·5 100 178	2·2 ±0·2 2·5 ±0·1 2·9 ±0·1	Anticentre	Extragalactic component removed
				40·5 100 178	2·0 ±0·2 2·65±0·1 2·9 ±0·1	North halo	
Korobkov (1964)	+56	35° by 25°	40, 25, 18·6, 13, 9·6	40 25 18 13 9 6	2·5 ±0·2 2·45±0·2 2·4 ±0·2 2·2 ±0·2 2·1 ±0·2 1·9 ±0·2	Towards spiral arm; $l = 98°$, $b = 5·3°$	Total emission
Costain (1960)	+50	40° by 15°	178, 38	85	2·35±0·04	Average all sky	Total emission
Adgie and Smith (1956)	+50	70° by 25°	378, 81·5, 38	81	2·5 ±0·1	North halo	Temperature difference
Parthasarathy and Lerfald (1965)	+65	60° by 60°	50, 30, 20, 10·5	10–30 30–50	2·0–2·28 2·6–2·77	North halo	Total emission
Ellis (1965)	−42	32° by 40°	9·6, 4·8, 2·3, 1·65	9·6	2·1	South pole	Total emission

in Table 1. The discrepancies between the indices quoted are significant and at least partly due to different assumptions made by each writer in the analysis of data. Turtle *et al.* assumed that the radio spectral index throughout the halo region was constant, and they used this assumption to separate out an extragalactic component of the received emission. The spectral data given by them refer to the "galactic" component only of the total emission. Parthasarathy and Lerfald, instead, assumed that the extragalactic component would be less than 10%, and they used this assumption as a basis for finding the spectral index variation across the halo.

It is apparent that the exact nature of the radio spectral law is by no means clearly defined.

It is the purpose of the present paper to give an analysis of a set of observations, some of which have been already reported (Wielebinski and Yates 1965; Yates and Wielebinski 1965), consisting of absolutely calibrated measurements of sky brightness, using scaled aerials, made at frequencies of 85, 48·5, 30, 20, and 14·1 MHz. The measurements were directed towards the zenith in Sydney, resulting in the observation declination $\delta = -34°$. No previous measurements have been made in this frequency range using scaled aerials directed at the southern halo region of the Galaxy.

II. Apparatus

(a) *Aerial Systems*

All observations were made at Fleurs Field Station, 50 km west of Sydney. For each frequency, the aerial was a single east–west oriented folded dipole 0·5 λ in length, suspended 0·25 λ above a λ by λ reflecting screen. The beamwidth between half-power points was 75° in the east–west plane and 115° in the north–south plane. The reflecting screen was constructed from overlapping pieces of 2 in. galvanized wire mesh laid directly onto the ground. Radiation from the ground can contribute to the aerial temperature. This can be either by direct pickup in the far-out side lobes where ground is subtended or else by penetration through the imperfect earth screen. A series of experiments was made at 85 MHz to determine the ground effects. To test the efficiency of the earth screen, the reflecting 2 in. mesh was replaced by a $\frac{1}{2}$ in. mesh. No change in aerial temperature greater than a random error was observed. To determine the contribution to the aerial temperature from ground subtended in the far-out side lobes, the aerial was relocated over an earth screen 6λ by 6λ in area. No temperature change was observed. In a final test, the aerial and screen were raised 0·2 λ above the ground, again giving no observable temperature change. These negative results are in agreement with similar experiments of Korobkov (1964) and Parthasarathy and Lerfald (1965), who found the temperature error due to the ground, with similar screens, to be less than 2%.

The aerials at 14·1, 20, and 30 MHz were matched to a balanced impedance of $(300+j0)\,\Omega$. A common 4 : 1 broad-band low-loss balun transformer was used at each of the three lowest frequencies. At 85 and 48·5 MHz, the aerials were matched to $(250+j0)\,\Omega$ and used with a 4 : 1 cable balun. An estimate was made of the loss in the balun used at each frequency by measuring the insertion loss in an unbalanced

system of two similar baluns back to back. The loss factors of the balanced lines used in the matching transformers were determined at each frequency by means of insertion loss measurements and by computation from the admittance of a short-circuited line of known length. A calculation was made of the standing waves on the balanced lines, using impedance measurements, and losses in the matching transformers were calculated. These results are tabulated, together with the balun losses, in Table 2. The impedance bandwidth of each aerial was measured, and in each case the standing wave ratio (SWR) was found to be less than 1·02 in the range $0{\cdot}99 f_0 < f < 1{\cdot}01 f_0$, where f_0 is the nominal frequency.

TABLE 2

LOSSES IN AERIAL SYSTEMS

Frequency (MHz)	Loss in Balun (dB)	Loss in Balanced Matching Transformer (dB)
85	0·1	0·05
48·5	0·08	0·06
30	0·1	0·08
20	0·2	0·1
14·1	0·15	0·12

(*b*) *Matching*

Mismatches on the balanced side of the balun introduce an unknown additional loss in the balun and cause a further loss due to enhanced standing waves on the aerial feed line. The impedance of an aerial changes slightly with temperature and weather conditions, and it is of interest to know the magnitude of the change in losses caused by these natural impedance variations. For this purpose, a series of tests was performed on the 48·5 MHz aerial in which mismatches were introduced by means of the balanced matching transformer.

The test was carried out during the transit of minimum of sky temperature, when incident power remains constant for some hours. For each mismatch, the feed line SWR was measured and the difference in power incident at the receiver between matched and mismatched cases noted. From this test, it was apparent that actual losses due to mismatch were even less than those computed. Power incident at the receiver was reduced by 1% for an SWR measured at the receiver of 1·2. Since, under normal conditions, natural variations in the impedance of the aerial did not cause an SWR in excess of 1·2, no variable matching was provided, except for measurements at 85 MHz.

The effect on the receiver noise of the impedance seen at its input was investigated by adding an additional quarter-wavelength to the aerial feed cable and noting changes in the receiver output. At all frequencies, except 85 MHz, the resulting changes were negligible. At this frequency, an initial difference of 50°K was measured with an SWR of 1·2 at the centre of the band, but this effect was eliminated with the

addition of a further unbalanced matching unit between the balun and the aerial feed cable.

(c) *Receiving Equipment*

The receiver was a switched radiometer that produced an output proportional to the power difference between the noise from the aerial and that from a resistive load at constant temperature of the same impedance as the aerial. Table 3 gives a summary of the characteristics of the receivers used at each frequency. In the receivers for the two highest frequencies, a low-noise preamplifier was followed by a mixer and 30 MHz i.f. amplifier. At all other frequencies, the low-noise preamplifier was followed by a standard communications receiver.

TABLE 3

SUMMARY OF RECEIVER CHARACTERISTICS

Frequency (MHz)	Bandwidth	Input Impedance (ohm)	Time Constant (sec)	Noise on Record (degK r.m.s.)
85	0·4 MHz	50	1	8
48·5	0·3	50	1	30
30	0·2	75	1	80
	8 kHz	75	4	180
20	8	75	4	600
14·1	8	75	4	1200

(d) *Calibration Standard*

The standards of noise power for measurements at all frequencies were temperature-limited diodes, type CV 2398. At the two highest frequencies, a diode was used with a 50 Ω load to produce a maximum temperature of 25 400°K. At the other frequencies, a diode with a 75 Ω load produced a maximum temperature of 38 000°K. At the two lowest frequencies, this was well below the aerial temperature, and, for this reason, calibration was made against an attenuated aerial signal. At 14 MHz, a 9 dB calibrated 75 Ω attenuator was inserted in the aerial line. At 20 MHz, a 6 dB calibrated 75 Ω attenuator was used. For calibration at each frequency, the noise generator was exactly matched by adding small lumped components across the diode load.

For our present purpose of determining the spectral index, it is essential to be able to measure accurately only the ratio of noise powers at different frequencies. The quantity I_1/I_2, where I_1 and I_2 represent the anode currents of the calibrating diode at the two different frequencies, will be equal to the noise power ratio, provided that the noise power output of the diode is accurately linear with anode current. A check was made on the linearity of the calibrating diode used by constructing a second noise generator, using two CV 2398 diodes in parallel, and comparing the outputs of the two generators for the same total current. It was found from this experiment that noise output from the calibrating source used was linear with current

to within 1% up to 60 mA and to within 2% to 85 mA. Absolute accuracy of the calibration at 85 MHz was determined to be within 3% by comparison with a 50 Ω thermal load at different temperatures.

III. Measurement Technique

Observations were conducted over the period June 1964 to June 1965. For all except the two highest frequencies, observations at each frequency were carried out over two separate months six months apart in order to allow the entire 24 hr of right ascension to be observed at night. Throughout the program, the observer calibrated the receiver every 2 hr and monitored the aerial impedance and interference.

The calibration procedure consisted of replacing the aerial at the aerial end of the feed cable by the noise generator and determining the noise-diode current required to produce the same deflection as the aerial. On occasions when the aerial line SWR exceeded 1·2, measurements were discontinued. This was normally due to very heavy condensation on the aerial and matching transformer. Interference was serious only in the pre-midnight summer observations at 14·1 MHz. On such occasions, the observing frequency was shifted slightly to locate a free band. At least five calibrated readings were obtained at each hour of right ascension for each frequency. Results were consistent from night to night to within 3% for observations on all frequencies, except 14·1 MHz where ionospheric effects gave occasional absorption.

IV. Results

(a) *Correction for Losses*

1. *Ionosphere*

The ionosphere seriously affects intensity measurements at frequencies below 20 MHz. The two separate phenomena that need to be considered are absorption in the F layers and the "iris" effect.

Since all observations were carried out at night, D layer absorption was avoided. Ellis (1963) has made a theoretical investigation of absorption in the F layer based on profiles obtained from free electron backscatter observations. His results agree well with extinction curves determined experimentally by Mitra and Shain (1953) and by Steiger (1961). During the period of observation at 14·1 MHz, night-time values of the critical frequency $f_0 F_2$ obtained from Camden, 15 km distant, were almost always less than 4 MHz. Theoretical considerations indicated a maximum loss of 0·1 dB for the ionospheric conditions experienced. For the 14·1 MHz observations, the highest value of sky temperature observed for each hour of right ascension was regarded as the closest approximation to the true sky temperature at that hour.

The "iris" effect produces, at a frequency f, total reflection of cosmic emission for zenith angles χ where

$$\chi > \cos^{-1}(f_0 F_2 / f).$$

At such angles, the earth temperature of 300°K is reflected into the aerial beam. Computation showed the iris effect to be negligible at 14·1 MHz for the highest value of $f_0 F_2 = 6$ MHz experienced during the investigations.

2. *Losses in the Aerial Systems*

Losses in the matching transformers and baluns at each frequency are tabulated in Table 2. No corrections were made for ground absorption on the basis of experimental measurements already described.

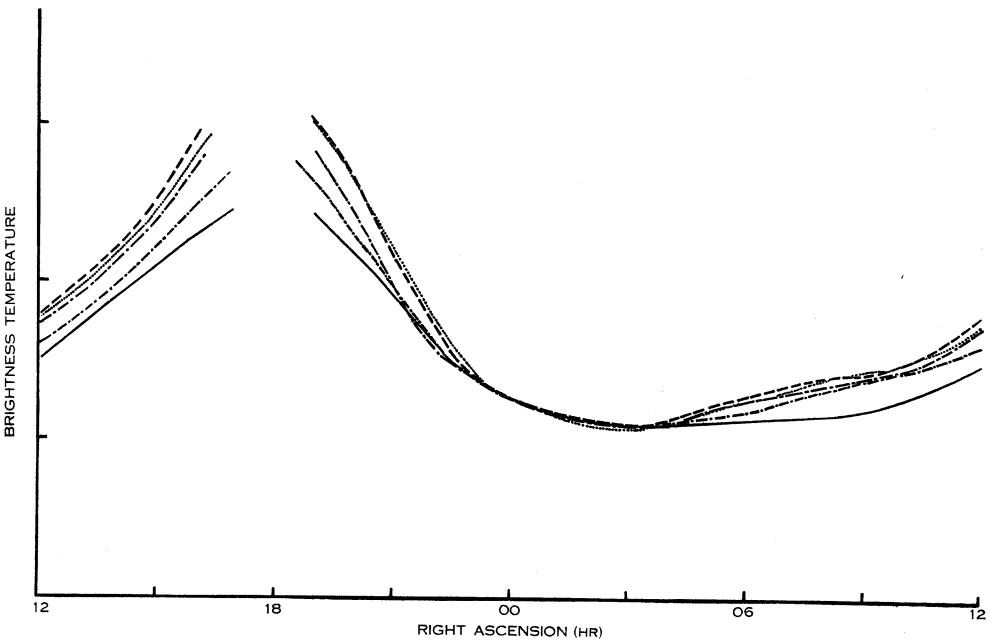

Fig. 1.—Brightness temperatures measured at each frequency plotted against right ascension ($\delta = -34°$). Values at 0040 hr in units of 10^3°K are given in parentheses with identification of curves as follows:

– – – 85 MHz (1·21); · · · · 48·5 MHz (5·14); —·—· 30 MHz (17·4);
–·–·– 20 MHz (54·8); —— 14·1 MHz (125·3).

(*b*) *Accuracy*

The maximum error in the measured values of absolute intensity was $\pm 7\%$. This value was derived from estimates of contributions of several individual sources of error. The major limitations to precision are the error in the absolute thermal calibration of the noise diode and the uncertainties in the exact magnitude of the calculated loss factors. The error in absolute intensity consists of two components, one dependent on and one independent of frequency. One component of the frequency-independent error is a ground effect, which, if present, would produce a constant loss factor over the relevant frequency range. Since spectral index is determined from a ratio of two intensities only, the frequency-dependent error in the absolute values of intensities will contribute to the error in the derived spectral index. We have assigned a value of $\pm 5\%$ for the value of frequency-dependent error, and, accordingly, the range of values of each spectral index given corresponds to the highest and lowest values consistent with a $\pm 5\%$ range in the values of intensity.

(c) *Results*

Brightness temperatures measured at each frequency are plotted in Figure 1. The temperatures were obtained after scaling all records at each sidereal hour, averaging, and applying a correction for the losses according to the values given in Table 2. Observations at 14·1 MHz between 07 and 10 hr R.A. were made close to sunset. It is possible that for these observations some attenuation of the radiation occurred in the ionospheric D layer.

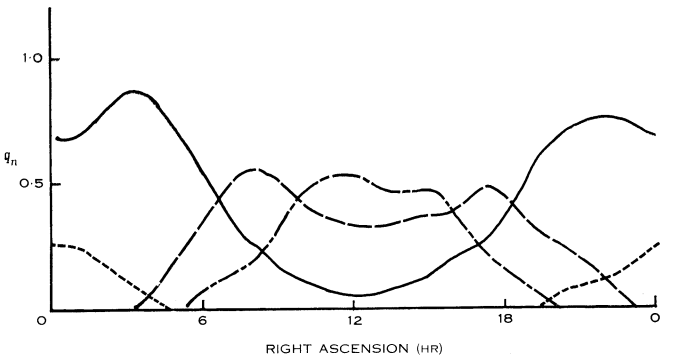

Fig. 2.—Computed values of the quantity q_n determined for the aerial used in the present experiment. —— $n = 1$, southern halo, $20° < -b^{II} < 60°$; — — $n = 2$, disc, $|b^{II}| < 20°$; —·—· $n = 3$, northern halo, $20° < b^{II} < 60°$; ····· $n = 4$, south pole, $-b^{II} < 60°$.

V. Analysis

(a) *Introduction*

Before we proceed with the interpretation of the aerial temperatures observed at each hour, let us consider the significance of aerial temperatures measured with an aerial whose beam covers several different emitting regions. We can express aerial temperature at any time as

$$T_a = \Sigma q_n T_n ,$$

where

$$q_n = \iint_n \bar{A}(\theta, \phi)\, \mathrm{d}\theta\, \mathrm{d}\phi$$

and T_n is the equivalent black-body temperature of radiation coming from the direction of the nth emitting region, averaged over that region; q_n is the normalized effective area integrated over all θ and ϕ contained in n. The values of q_n can be determined for any set of emitting regions and aerial pattern. In Figure 2, the q_n are shown for the aerial used in the present experiment with a division of the sky into four radiating regions corresponding to directions of distinct regions of the Galaxy. However, to determine the dominant component in the received power at

any one time, it is necessary to know the relative temperatures of the regions. If we assume that temperature observed in any one direction is proportional to the extent of the emitting region measured along the line of sight, we can define a set of p_n such that

$$p_n = q_n T_n \propto \iint_n \bar{A}(\theta, \phi)\, k_n(\theta, \phi)\, \mathrm{d}\theta\, \mathrm{d}\phi\,,$$

where $k_n(\theta, \phi)$ is the extent of the nth source region measured in the direction (θ, ϕ). Ideally, we can obtain values of p_n for all regions and thus determine the relative contribution to the aerial temperature of each emitting region for each hour of right ascension. It is apparent that if the different regions have different emission spectra, then a knowledge of the p_n is necessary for the complete interpretation of the observed spectra.

(*b*) *Analysis*

The method of reducing experimental observations and the interpretation that we make of them are dependent on our model of the Galaxy. Assumptions concerning the changes of the spectral index law with the location of the source of emission are of particular importance. We have the choice either of making severe assumptions in order to produce a model that is sufficiently simple to allow precise analyses or of adopting a more realistic model, being satisfied with a less detailed interpretation. Both types of analysis are useful in setting limiting values to certain parameters, such as, in the present case, the spectral index of galactic radio emission and the magnitude of extragalactic emission.

Let us now consider two possible models, which we will later use as a basis for our analysis.

Model A. In the frequency range of interest, the power spectral law $\alpha(\lambda)$ is independent of the origin of the emission throughout the Galaxy.

Model B. Significant differences exist between the spectral laws of radio emission originating in the disc region and of that originating in the halo region.

In each model, we will allow the possibility of a uniform extragalactic component with a different spectral law from that of galactic emission. In addition, we will postulate that absorption in ionized hydrogen clouds significantly affects the aerial temperature between 07 and 09 hr and between 15 and 19 hr R.A. only. These rather arbitrary limits are justified by the narrow-beam surveys of Shain (1957) and Ellis (1964), which show that absorbing regions lie within 10° of the galactic plane at 14 MHz. A consideration of Figure 2 indicates that the contributions to the aerial temperature of radiation from within 10° of the galactic plane is dominant only for the ranges of right ascension that we have suggested.

(*c*) *Analysis on the Basis of Model A*

In this model, we have made a sufficiently severe assumption to be able to separate galactic from extragalactic emission and to compute values for the galactic radio spectral index and the intensity of extragalactic emission associated with the

model. The analysis is similar to that of Turtle *et al.* (1962). At any particular time, and for each frequency, we can say that the two contributions to the aerial temperature are T_G, due to emission from the Galaxy, and T_0, which is the component inde-

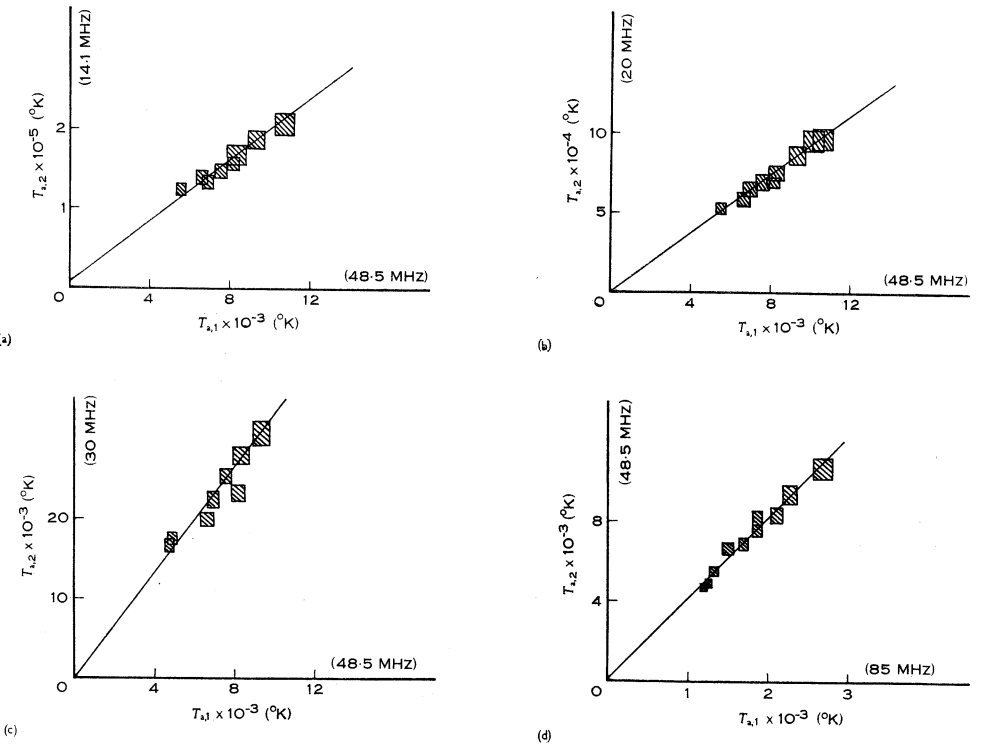

Fig. 3.—Temperatures observed at each frequency compared with those observed at 48·5 MHz. Each point (shaded square indicates 5% possible error) corresponds to a particular value of right ascension. The slope of the straight line of best fit is the quantity n_{12}.

pendent of direction equal to the integrated extragalactic emission. Thus, for aerial temperature T_a at frequency f_1, we write

$$T_{a,1} = T_{G,1} + T_{0,1}$$

and, for a second frequency f_2,

$$T_{a,2} = T_{G,2} + T_{0,2}\,.$$

Since, in this model, spectral law is independent of direction, we can say that

$$\frac{T_{G,2}}{T_{G,1}} = n_{12}\,,$$

where n_{12} is a constant independent of direction. Similarly,

$$\frac{T_{0,2}}{T_{0,1}} = n_{0,12}\,,$$

that is,

$$T_{a,2} = n_{12}(T_{G,1}+T_{0,1})+(n_{0,12}-n_{12})T_{0,1} .$$

If we plot $T_{a,1}$ against $T_{a,2}$, we will obtain a straight line of slope n_{12}, with intercept on the $T_{a,2}$ axis of $(n_{0,12}-n_{12})T_{0,1}$.

In Figure 3, observed aerial temperatures at 48·5 MHz are plotted against those observed at other frequencies, for each hour of sidereal time except those in which we have assumed absorption to be significant. The squares indicate the 5% error applicable for spectral determination. Since, on the basis of this model, the

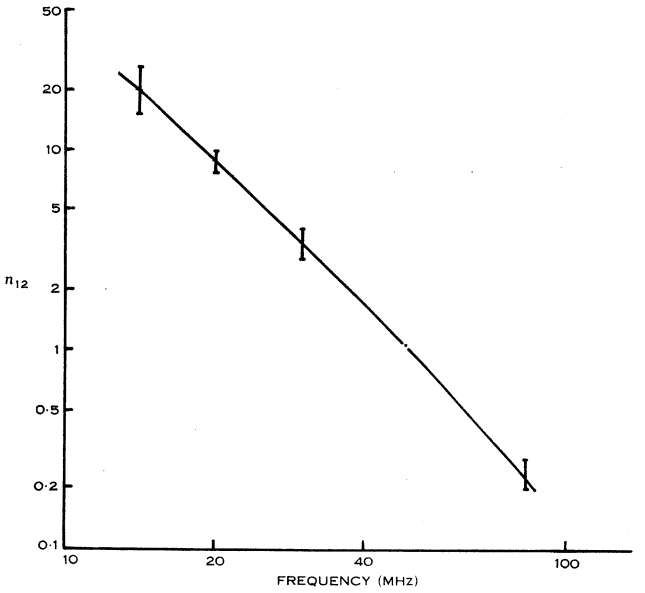

Fig. 4.—Determination of the spectral law—the quantity n_{12} for $f_1 = 48·5$ MHz plotted as a function of frequency.

two-frequency temperature plots must yield straight lines, we are justified in drawing straight lines of best and limiting fit in order to yield median and limit values of n_{12}. We can now use the values of n_{12} obtained from the two-frequency temperature plots to determine the spectral law. In Figure 4, the values of n_{12} corresponding to $f_1 = 48·5$ MHz are plotted against frequency.

In Figure 5, corresponding values of brightness relative to 48·5 MHz are shown, together with curves representing maximum, median, and minimum frequency dependence of the spectral index consistent with the five measured points. Table 4 presents the values of power spectral index determined from analysis of our experimental data on the basis of Model A for several different frequencies. The range of values given corresponds with the limiting curves shown in Figure 5.

Magnitude of the Extragalactic Component

For the model being discussed, the intercepts on the low frequency axis of the two-frequency temperature plots represent the quantity $(n_{0,12}-n_{12})T_{0,1}$. In each case,

we can plot the value of T_0 corresponding to several assumed values of the extragalactic temperature spectral index β_0 consistent with the size of the intercept obtained. Figure 6 is a T_0 versus β_0 plot for the intercepts from the $T_{a,85}$–$T_{a,20}$ and $T_{a,85}$–$T_{a,14}$

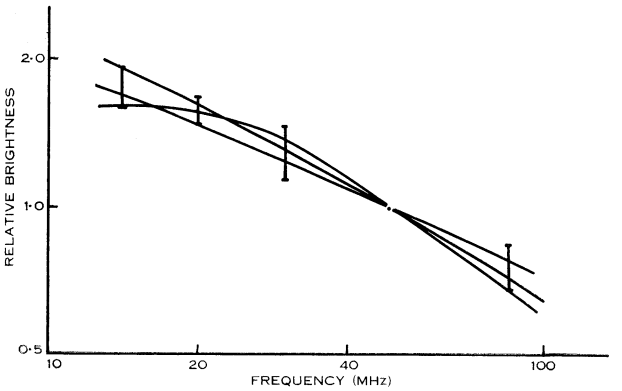

Fig. 5.—Values of brightness relative to brightness at 48·5 MHz as a function of frequency, determined from the n_{12} shown in Figure 4. Curves of maximum, median, and minimum variation of spectral index are shown.

plots shown in Figure 7. Superimposed is a similar curve for the $T_{a,48}$–$T_{a,14}$ intercept scaled to represent T_0 at 85 MHz. The shaded area indicates the intersection region of the three curves for the error ranges applicable. The maximum possible values of

TABLE 4

VALUES OF POWER SPECTRAL INDEX

Determined from analysis of experimental data on basis of Model A

Frequency (MHz)	Power Spectral Index α
60	$0{\cdot}51^{+0{\cdot}15}_{-0{\cdot}05}$
39	$0{\cdot}51^{+0{\cdot}15}_{-0{\cdot}05}$
25	$0{\cdot}4 \pm 0{\cdot}2$
17	$0{\cdot}3 \pm 0{\cdot}2$

$T_{0,85}$ for each assumed value of β_0 derived from the shaded area of Figure 6 are given in Table 5, together with parallel results of Shain (1959) and Turtle *et al.* (1962). As a check to our estimates, we can compute the size of the intercepts for the $T_{a,48}$–$T_{a,20}$, $T_{a,48}$–$T_{a,30}$, and $T_{a,85}$–$T_{a,48}$ plots. The maximum values for these intercepts are 1500°K, 250°K, and 130°K, which would produce negligible intercepts, in

agreement with the actual plots shown in Figure 3. We note that it has been assumed that β_0 is independent of frequency down to 14 MHz.

We have also made no allowance for the component of the measured temperature due to ground radiation. Turtle *et al.* (1962) have shown that the ground contribution reduces the low frequency axis intercept by $(pT_g n_{12})$°K, where p is the ground absorption factor and T_g is the ground temperature. Even allowing for a 5% ground loss factor, the reduction in the intercept for the $T_{a,48}$–$T_{a,14}$, $T_{a,85}$–$T_{a,20}$, and $T_{a,85}$–$T_{a,14}$ plots would be less than 6% in each case.

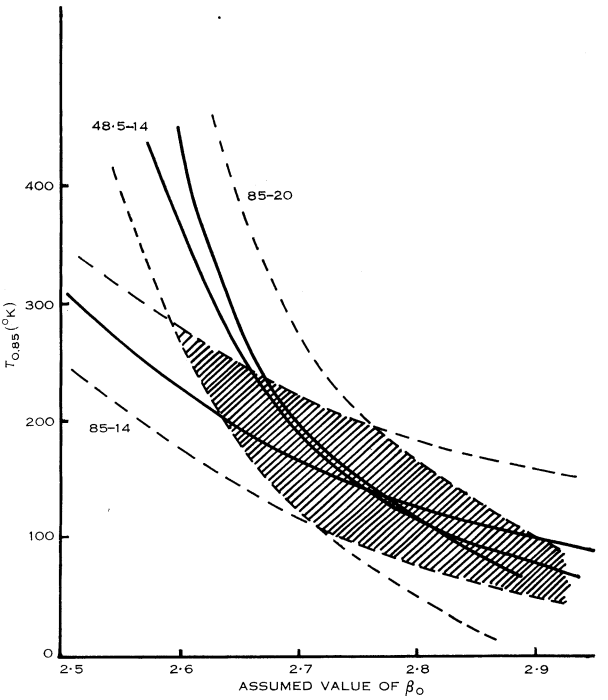

Fig. 6.—Determination of magnitude of the extragalactic component of emission at 85 MHz for a range of assumed values of its temperature spectral index.

Implications of Model A

A constant value of $\alpha(\lambda)$ throughout the Galaxy raises some difficulties in interpretation of observed spectra in terms of synchrotron emission theory. This model requires either great uniformity of magnetic fields, electron energies, and density throughout the Galaxy or else very fortuitous conditions. Ginzburg and Syrovatskii (1965) show that, if the energy spectrum of ultra-relativistic electrons is represented by the expression

$$n(E) \propto E^{-\gamma} \mathrm{d}E ,$$

then the main contribution to emission of frequency f is from electrons within the energy range

$$E_1 < E < E_2 ,$$

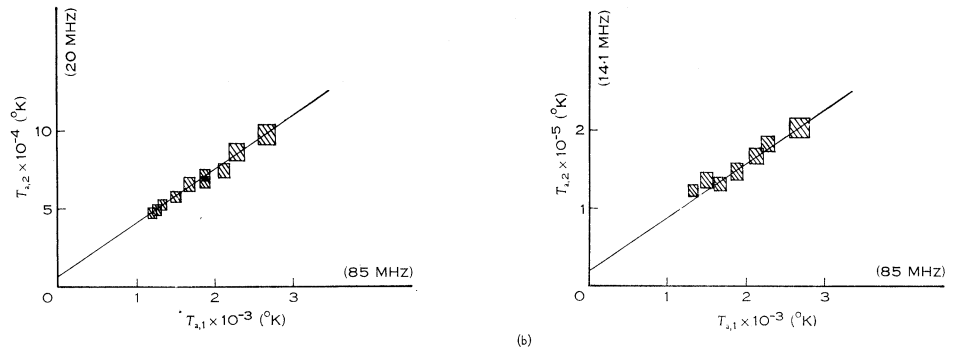

Fig. 7.—Further set of two-frequency brightness plots, showing measurable intercepts on the low frequency axes which are used in evaluating the extragalactic component (shaded squares indicate 5% possible error).

TABLE 5

EXPERIMENTAL DETERMINATIONS OF THE EXTRAGALACTIC COMPONENT OF SKY EMISSION

Temperature Spectral Index β_0	$T_{0,85}$ (°K)		
	Present Results	Turtle *et al.* (1962)	Shain (1959)
2·6	300	240–520	210–440
2·7	130–250	210–380	190–380
2·8	80–160	150–260	170–330
2·9	40–110	110–220	140–290

where

$$E_1 = mc^2\left(\frac{4\pi mcf}{3eH\,y_1(\gamma)}\right)^{\frac{1}{2}},$$

$$E_2 = mc^2\left(\frac{4\pi mcf}{3eH\,y_2(\gamma)}\right)^{\frac{1}{2}},$$

with $y_1(\gamma)$ and $y_2(\gamma)$ as tabulated by Ginzburg and Syrovatskii. If the value of γ is constant over the range of energies that contribute to the emission at a particular frequency, the value of α at that frequency is given by

$$\alpha = \tfrac{1}{2}(\gamma - 1).$$

If we take as values for magnetic field variation across the Galaxy 5×10^{-5} G for the disc and 5×10^{-6} G for the distant halo (Sciama 1962), then a threefold change in the energy of ultra-relativistic electrons is required to produce emission at the same frequency as we change direction of observation. Model A thus requires a constant

γ over at least a threefold range of the spread of energies that contribute to radiation at one frequency. However, such a condition also requires a constant value of α over a tenfold frequency range in any particular direction, which is not supported by experiment.

Very few high resolution studies have been made of the change of spectrum across the halo region, so it is difficult to produce direct experimental evidence to invalidate Model A. Komesaroff (1961) found some variation in spectral index looking in different directions close to the galactic plane, but the variation was within the error limit given.

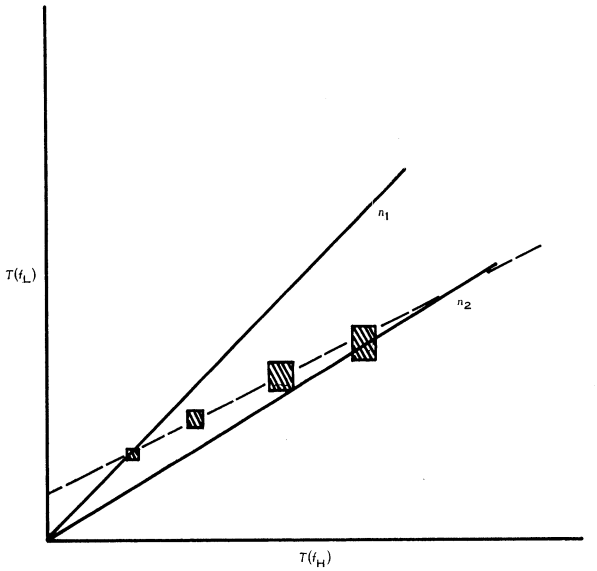

Fig. 8.—Two-frequency temperature plot for Model B (shaded squares indicate 5% possible error). The actual curve will osculate the lines of slope n_1 and n_2. The possibility of erroneous interpretation is indicated. (f_H means the higher frequency, f_L the lower.)

(*d*) *Analysis on the Basis of Model B*

In this model, we allow for a difference in the spectra of emission originating in different regions. Let us assume initially that galactic emission has two distinct components, one with power spectrum $\alpha_1(\lambda)$ and the other with power spectrum $\alpha_2(\lambda)$. In this case, the method of plotting $T(f_1)$ against $T(f_2)$ would produce points lying along a curve osculating lines of slope n_1 and n_2, where n_1 and n_2 are the temperature ratios corresponding to $\alpha_1(\lambda)$ and $\alpha_2(\lambda)$ respectively. This is illustrated in Figure 8. If an extragalactic component is present in the emission, then the tangents of slope n_1 and n_2 will be displaced along the low frequency axis by distances $(n_e-n_1)T_0$ and $(n_e-n_2)T_0$ respectively, n_e referring to the extragalactic component. This is illustrated in Figure 9. Since we are no longer justified in drawing a straight line through the measured points, two-frequency temperature plots yield no information about the extragalactic component when Model B is assumed. Figure 8 shows

how an erroneous value for the extragalactic component can be determined if the assumption of Model A, with its method of analysis, is invalid. At this stage in the analysis, we must either set up a more detailed model for the distribution of emission

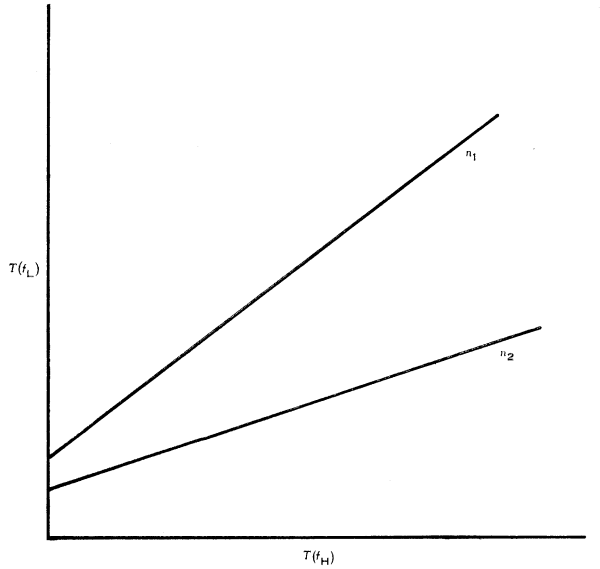

Fig. 9.—Two-frequency temperature plot, as in Figure 8, including effect of extragalactic emission.

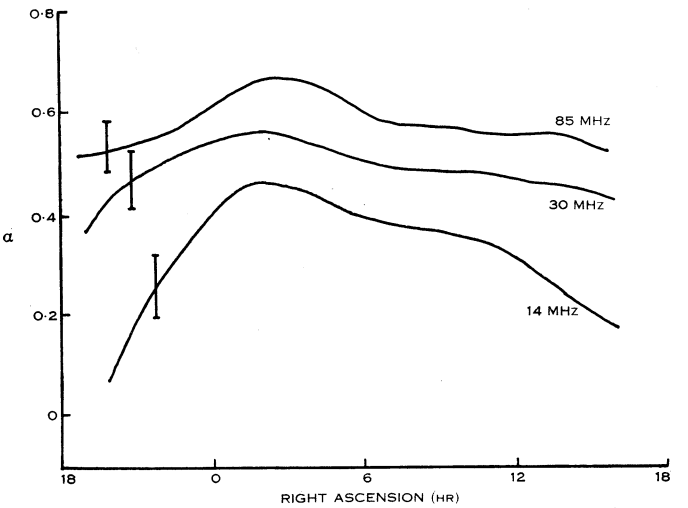

Fig. 10.—Variation with right ascension of power spectral index of total received emission.

with different spectral indices, and compute the p_n referred to in part (*a*) of this section, or proceed with a study of the sky brightness spectrum, making no attempt to distinguish the galactic and extragalactic components. Since the necessary

information required to determine the p_n is not available, we must follow the latter course. In this case, the most useful method of presentation of data is in the form of spectral curves for each hour of right ascension. From these data we can state that, at any given frequency, the highest α, denoted by α_H, observed over the 24 hr of right ascension is such that

$$\alpha_H < \alpha_{max},$$

where α_{max} is the highest spectral index of any emission region in the sky at that frequency. Similarly, we can say that

$$\alpha_L > \alpha_{min}.$$

For each hour of right ascension, curves of best fit were plotted using the sky temperatures at each frequency. From these curves, it was possible to determine the change of spectral index with right ascension at any frequency between 85 and 14 MHz. In Figure 10, we reproduce the power spectral index versus right ascension curves for the limiting cases of 85 and 14 MHz and for 30 MHz. In Table 6, maximum and minimum values of power spectral index α, determined from an analysis of our experimental data on the basis of Model B, are presented.

TABLE 6

RANGE OF VARIATION OF POWER SPECTRAL INDEX OF TOTAL RECEIVED EMISSION FOR ALL RIGHT ASCENSIONS

Determined from analysis of experimental data on basis of Model B

Frequency (MHz)	Range of Observed α
85	0·7 –0·5
30	0·58–0·45
14	0·45–0·15

VI. DISCUSSION

We have analysed a set of experimental results to derive

(i) the magnitude of the extragalactic component of emission associated with a model of the Galaxy in which radio emission has a universal spectral law;

(ii) limiting values for the radio spectral index variation across the sky in the frequency range 14–85 MHz.

It is of interest now to relate our own results to those of other observers, in order to develop a picture of the intensity variation of galactic radio emission over a wide frequency range which will enable theoretical models to be tested. Because of

the multiplicity of observing directions and beamwidths used, it is much more meaningful to compare the slopes (or spectral indices) of intensity curves than their absolute values. In Figure 11, we have shown the range of power spectral indices observed over all directions by some of the experimenters listed in Table 1. Included on the diagram are our own results for each of the models adopted.

There remains some doubt as to the high frequency asymptote of the index. Our own results support the value of 0·6 derived by Komesaroff (1961) and adopted by Lequeux (1965), whereas both Turtle *et al.* (1962) and Parthasarathy and Lerfald (1965) favour a value approaching 0·9. There appears to be quite good agreement between our own results and those of Korobkov (1964), indicating that the range of spectral indices observed in the southern halo region is not significantly different from

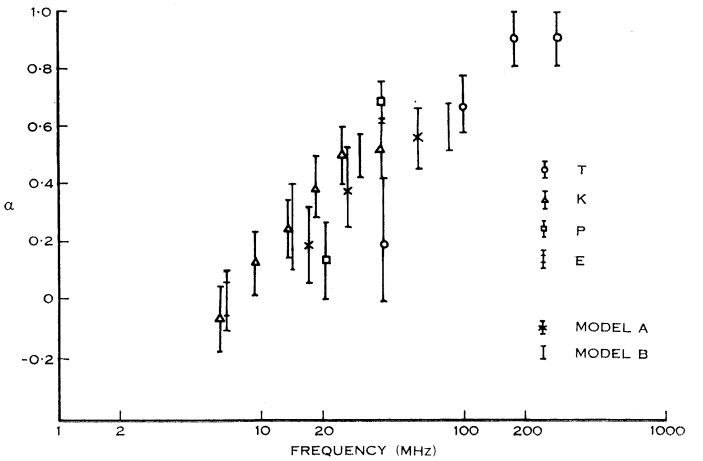

Fig. 11.—Results of scaled aerial experiments, showing the range of power spectral indices observed over all directions. T: Turtle *et al.* (1962); K: Korobkov (1964); P: Parthasarathy and Lerfald (1965); E: Ellis (1965).

that observed in the north. Very few measurements have been made of the extragalactic component of total sky emission. Our own results are shown in Table 5, together with values obtained by Shain (1959) and Turtle *et al.* (1962). The results of the latter were based on data from a similar scaled aerial experiment. The estimates given by Shain were derived from observations at 19·7 MHz of the total absorption of extragalactic emission in an HII region, 30 Doradus, in the Large Magellanic Cloud. Although the method used by Shain is superior, the accuracy of his results is limited by uncertainty as to the exact size of 30 Doradus.

Scaled, narrow-beam, absolute surveys at frequencies both above and below 100 MHz are required before detailing the variation of spectral law across the Galaxy, and the value of the high frequency asymptote, can be obtained. We are at present engaged in repeating measurements at the same frequencies with scaled aerials of medium resolution.

VII. Acknowledgments

This work is part of the research program of the School of Electrical Engineering at the University of Sydney. One of us (K.W.Y.) has been supported by a Commonwealth Studentship.

We wish to thank Professor B. Y. Mills of the School of Physics for useful discussions.

VIII. References

Adgie, R., and Smith, F. G. (1956).—*Observatory* **76**: 181.
Costain, C. H. (1960).—*Mon. Not. R. Astr. Soc.* **121**: 413.
Ellis, G. R. A. (1963).—*Aust. J. Phys.* **16**: 411.
Ellis, G. R. A. (1964).—*Nature* **204**: 272.
Ellis, G. R. A. (1965).—*Mon. Not. R. Astr. Soc.* **130**: 429.
Ginzburg, V. L., and Syrovatskii, S. I. (1965).—*A. Rev. Astr. & Astrophys.* **3**: 297.
Komesaroff, M. M. (1961).—*Aust. J. Phys.* **14**: 515.
Korobkov, Yu. S. (1964).—*Izv. Vyssh. Ucheb. Zaved. Radiofiz.* **7**: 982.
Lequeux, J. (1965).—*Annls Astrophys.* **28**: 360.
Mitra, A. P., and Shain, C. A. (1953).—*J. Atmos. Terr. Phys.* **4**: 204.
Parthasarathy, R., and Lerfald, G. M. (1965).—*Mon. Not. R. Astr. Soc.* **129**: 395.
Sciama, D. W. (1962).—*Mon. Not. R. Astr. Soc.* **123**: 317.
Shain, C. A. (1957).—*Aust. J. Phys.* **10**: 195.
Shain, C. A. (1959).—Symp. IAU No. 9 (Paris 1958). p. 328.
Steiger, H. J. (1961).—*J. Geophys. Res.* **66**: 51.
Turtle, A. J., Pugh, J. F., Kenderdine, S., and Pauliny-Toth, I. I. K. (1962).—*Mon. Not. R. Astr. Soc.* **124**: 297.
Wielebinski, R., and Yates, K. W. (1965).—*Nature* **205**: 581.
Yates, K. W., and Wielebinski, R. (1965).—*Nature* **208**: 64.